Available online at www.sciencedirect.com
ScienceDirect
Catalysis Today 131 (2008) 314–321
CATALYSIS TODAY
www.elsevier.com/locate/cattod

Ti-modified alumina supports prepared by sol–gel method used for deep HDS catalysts

Weiqiang Huang [a], Aijun Duan [a], Zhen Zhao [a,*], Guofu Wan [a], Guiyuan Jiang [a], Tao Dou [b], Keng H. Chung [c], Jian Liu [a]

[a] *State Key Laboratory of Heavy Oil Processing, China University of Petroleum, Beijing 102249, PR China*
[b] *Key Laboratory of Catalysis, China University of Petroleum, Beijing 102249, PR China*
[c] *Syncrude Canada Ltd., 9421-17 Avenue, Edmonton, Alberta, Canada T6N 1H4*

Available online 26 November 2007

Abstract

The typical physico-chemical properties and their hydrodesulfurization activities of NiMo/TiO_2-Al_2O_3 series catalysts with different TiO_2 loadings were studied. The catalysts were evaluated with a blend of two kinds of commercially available diesels in a micro-reactor unit. Many techniques including N_2-adsorption, UV–vis DRS, XRD, FT-Raman, TPR, pyridine FT-IR and DRIFT were used to characterize the surface and structural properties of TiO_2-Al_2O_3 binary oxide supports and the NiMo/TiO_2-Al_2O_3 catalysts. The samples prepared by sol–gel method possessed large specific surface areas, pore volumes and large average pore sizes that were suitable for the high dispersion of nickel and molybdenum active components. UV–vis DRS, XRD and FT-Raman results indicated that the presence of anatase TiO_2 species facilitated the formation of coordinatively unsaturated sites (CUS) or sulfur vacancies, and also promoted high dispersion of Mo active phase on the catalyst surfaces. DRIFT spectra of NO adsorbed on the pure MoS_2 and the catalysts with TiO_2 loadings of 15 and 30% showed that NiMo/TiO_2-Al_2O_3 catalysts possessed more CUS than that of pure MoS_2. HDS efficiencies and the above characterization results confirmed that the incorporation of TiO_2 into Al_2O_3 could adjust the interaction between support and active metals, enhanced the reducibility of molybdenum and thus resulted in the high activity of HDS reaction.

Keywords: Sol–gel method; TiO_2-Al_2O_3 binary oxides; Characterization; NiMo catalysts; Hydrodesulfurization

1. Introduction

Increasing awareness of the impact of environmental pollution from automobiles has drifted the responsibility of pollution control to the refiners. In view of diesel fuels as an important transportation power, the reduction of the sulfur content in diesel is one of the primary goals of the recently proposed regulations by the Directive of the European Parliament and the Environmental Protection Agency (EPA). And the sulfur content is expected to be lowered to 10–50 $\mu g\ g^{-1}$ level in the most of developed countries and developing countries by the end of this decade. The current USA specification of sulfur in diesel is 15 $\mu g\ g^{-1}$ and it is expected to be 10 $\mu g\ g^{-1}$ in 2008 in Europe [1,2]. As a consequence, zero-emission and zero S fuels are expected in the near future. The desulfurization technologies have become the effective choices to meet the ultra low-sulfur fuel specifications, whereas the conventional hydrodesulfurization (HDS) processes cannot currently produce ultra low-sulfur level diesel fuels, therefore, the essential approaches are the designs and developments of active HDS catalysts with better activity.

The catalyst supports play important roles on promoting the dispersion of the active components and altering the catalytic functionalities through metal–support interaction (MSI) [3,4]. Many kinds of materials have been tried as supports to Ni(Co)Mo(W) active components. TiO_2-supported systems exhibited higher activities compared to Al_2O_3 supports. In order to improve the disadvantages like limited thermal instability, low surface area and unsuitable mechanical properties of TiO_2, the combinations of TiO_2 with γ-Al_2O_3, ZrO_2 and SiO_2 supports are alternative promising approaches to modify the present γ-Al_2O_3 support [5,6].

* Corresponding author. Tel.: +86 10 89731586.
E-mail address: zhenzhao@cup.edu.cn (Z. Zhao).

0920-5861/$ – see front matter © 2007 Elsevier B.V. All rights reserved.
doi:10.1016/j.cattod.2007.10.029

Among the various composite oxide supports, more and more considerations are taken into account the combination of TiO_2 and Al_2O_3 because of the increased reducibility and sulfurability of Ti-containing catalysts, which are related to the fact that the redox processes of the active phases (Mo) are facilitated by the semiconductor character of TiO_2 compared with the pure insulating Al_2O_3 [7–11]. The modification of the surface of alumina with TiO_2 eliminates the most of reactive surface hydroxyl groups and avoids the formation of tetrahedral Mo oxide species, resulting in an increase of octahedral Mo active species and thus leading to a higher HDS activity [12–15].

Various methods have been employed to prepare titania-alumina support, involving coprecipitation, impregnation and chemical vapor deposition (CVD). In general, higher surface areas of binary oxides are obtained in these methods compared with TiO_2. Saih and Segawa et al. [16–20] prepared TiO_2-Al_2O_3 composite supports by CVD method using $TiCl_4$ as Ti precursor. They found that TiO_2-coated Al_2O_3 supports exhibited textural properties similar to those of alumina and surface properties similar to those of titania [17]. Mo oxide species supported on the composite carrier were better sulfided than on alumina and probably better dispersed than on titania, which led to an increase in the number of HDS active centers known to be coordinatively unsaturated sites. The industrial HDS tests of straight run distillate gas oil show that sulfide catalysts supported on TiO_2-Al_2O_3 composite (11 m%) could reduce the sulfur level of diesel fuel from 500 to 50 ppm under conventional hydrodesulfurization conditions. Saih and Segawa [20] also studied the physico-chemical properties and the HDS activities of NiMo/TiO_2-Al_2O_3 series of catalysts with different TiO_2 loadings. The specific surface area of the binary oxide was 216 $m^2\ g^{-1}$, and the pore volume was up to 0.70 mL g^{-1}. The HDS tests showed that the NiMo/TiO_2-Al_2O_3 catalysts were more active than NiMo/Al_2O_3 catalysts for the model compound HDS of DBT, 4-MDBT and 4,6-DMDBT. Ramírez et al. [21–24] have made many efforts to study the detailed characterization of hydrotreating catalysts supported on TiO_2-Al_2O_3 binary oxides and tried to explain the roles of Ti incorporation in supported Mo, CoMo, NiMo and NiW hydrodesulfurization catalysts. Several methods have been employed to prepare TiO_2-Al_2O_3 binary oxides, involving mixing boehmite with the required amount of a solution of titanium isopropoxide in isopropanol. The obtained TiO_2-Al_2O_3 binary oxides presented the good textural properties that the specific surface area exceeded 210 $m^2\ g^{-1}$, and the pore volume was 0.35 mL g^{-1} which was similar to that of pure alumina. And the HDS efficiencies of NiMo/TiO_2-Al_2O_3 were higher than that of NiMo/Al_2O_3 with the feedstock of Maya heavy crude [25].

The above researches confirmed the good performances of TiO_2-Al_2O_3 binary oxides in hydrodesulfurization, and the results also showed that TiO_2-Al_2O_3-supported catalysts showed higher activities compared with Al_2O_3 and/orAl_2O_3-SiO_2-supported catalysts. In this paper, a series of TiO_2-Al_2O_3 binary oxide support were prepared by sol–gel method using cheap inorganic pseudoboehmite as aluminum source, and the catalytic performances of these TiO_2-Al_2O_3 binary composite supported catalysts for HDS of diesel oil were investigated with the diesel feedstock to investigate the promoting effect of titanium modification on the HDS performance of catalysts. The exploration of sol–gel method and optimized preparation conditions in this work are expected to obtain TiO_2-Al_2O_3 composite with high specific surface area and suitable pore diameter as the support for deep hydrodesulfurizaiton with the feedstock of diesel oil.

2. Experimental

2.1. Feed properties

The feedstock was a 467.6 μg g^{-1} sulphur diesel which was a blend of two commercial available diesels from Fushun refinery. The properties of the diesel feedstock are shown in Table 1.

2.2. Catalyst preparation

TiO_2-Al_2O_3 binary oxides were prepared by sol–gel method with Tetra-*n*-butyl-titanate, ethanol, nitric acid, deionized distilled water and pseudoboehmite. Firstly, titanium sol was made from the Tetra-*n*-butyl-titanate, ethanol, nitric acid and deionized distilled water with the molar ratio of 1:15:0.3:3. Then the pseudoboehmite was dissolved with certain proportional ethanol and nitric acid at certain temperature under the gently stirring condition for hours until aluminum-sol generated. Then titanium-sol was dripped into the slurry under the drastic stirring condition to form the gel. And it was dried in air for 10 h at 380 K and calcined at 773 K for 6 h. The supports obtained were named as TiO_2-Al_2O_3-χ and NiMo/TiO_2-Al_2O_3-χ, respectively, where χ is equal to 1–7, representing the weight ratios of $TiO_2/(TiO_2 + Al_2O_3)$, i.e., 0, 5, 10, 15, 20, 25 and 30%.

The NiMo/TiO_2-Al_2O_3 catalysts were prepared by two-step impregnations of the supports with ammonium heptamolybdate and nickel nitrate solutions using the incipient wetness method. After the molybdenum impregnation step, the samples were dried at 383 K for 12 h, and calcined at 773 K for 4 h. The NiO and MoO_3 loadings were 3.5 and 15.5 m%, respectively.

Table 1
The typical physico-chemical properties of feedstock

Properties	Data
Density @ 20 °C/g cm^{-3}	0.8391
Sulfur (μg g^{-1})	467.59
Distillation (°C)	
IBP	154
10%	218
30%	258.2
50%	290
70%	316.1
95%	365
FBP	450.8

2.3. Catalyst characterization

The specific surface area and pore distribution of the catalyst samples were determined by BET method. X-ray powder diffraction (XRD) profiles were recorded in an XRD-6000 diffractometer using Cu Kα radiation under 40 kV, 30 mA, scan range from 20 to 80° at a rate of 4° min^{-1}. The UV–vis diffuse reflectance spectra (DRS) experiments were performed on Hitachi U-4100 UV–vis spectrophotometer with the integration sphere diffuse reflectance attachment. The powder samples were loaded in a transparent quartz cell and were measured in the region of 200–800 nm at room temperature. The standard support reflectance was used as the baseline for the corresponding catalyst measurement. Afterwards, H_2-TPR was carried out using 10% hydrogen in helium at a constant flow rate of 40 mL min^{-1}, from 333 to 1273 K, at a heating rate of 10 K min^{-1}. Laser Raman spectra were recorded by a Jobin-Yvon U-1000 Raman spectrometer with an Ar^+ laser; 488.0 nm and 200 mW were used. FT-IR of pyridine adsorption was conducted by the FT-IR spectrometer (BIO-RAD, FTS3000) equipped with an in situ cell containing CaF_2 windows. The Brönsted and Lewis acid sites could be distinguished by the bands of chemisorbed pyridinium ion at ~1540 cm^{-1} and coordinative bonded pyridine at ~1450 cm^{-1}, respectively. The band at 1490 cm^{-1} is usually associated with pyridine adsorbed on both Brönsted and Lewis acid sites. The surface structure of NiMo sulfided catalyst was characterized by means of diffuse reflectance infrared Fourier transform (DRIFT) measurements using NO as a probe molecule [26–28] to study the distribution of coordinatively unsaturated site. The catalysts were presulfided with a 2 m% CS_2-cyclohexane mixture under the conditions of Liquid Hourly Space Velocity (LHSV) of 1.0 h^{-1}, temperature of 593 K, total pressure of 4 MPa and a H_2/cyclohexane ratio of 600 mL mL^{-1} of CS_2, and were loaded in the IR shell and flashed He at 150 °C for 30 min, then cooled to room temperature. 0.4% NO/He mixture was flew into the sample for 30 min to reach the balance of NO adsorption, subsequently turned to He flow for 30 min. FT-IR spectra of NO were collected at intervals of 30 K from 303 to 473 K using FTS-3000 spectrophotometer manufactured by American Digilab company.

2.4. Catalytic activity measurement

Catalytic performance was evaluated in a high-pressure fixed-bed reactor with 2 g of catalyst (grain size of 0.3–0.5 mm). All catalysts were presulfided for 6 h with a 2 m% CS_2-cyclohexane mixture under the conditions of LHSV of 1.0 h^{-1}, temperature of 593 K, total pressure of 4 MPa and a H_2/cyclohexane ratio of 600 mL mL^{-1}. Hydrodesulfurization tests of diesel were carried out under the conditions of 623 K, 5.0 MPa, 600 mL mL^{-1} and 1.0 h^{-1}. Catalytic activities were measured at steady state after 13 h on-stream. The catalytic activity under investigation was estimated by the HDS efficiency.

3. Results and discussion

3.1. Specific surface area and pore volume

The results for the textural characterization and pore size distributions of oxide catalysts are presented in Table 2 and Fig. 1, and the properties of several sulfided catalysts after HDS reaction are shown in Table 3. From Table 2, it can be seen that the specific surface areas of the catalysts decrease with the increase of Ti loading, but not very significantly. The minimal specific surface area of this series of catalysts reaches 221.03 $m^2 g^{-1}$ when the TiO_2 loading is 20 m%, which is close to that of pure Al_2O_3-supported catalyst. The high surface area is favorable for the high and uniform dispersion of active components of nickel and molybdenum. The pore volumes and average pores of catalysts increase with the increasing of the TiO_2 loadings, and reach a maximal value, then decrease with the further increase in TiO_2 loadings. Deng et al. [26] believed that the distribution of TiO_2 over Al_2O_3 surface possessed a maximum value as 0.079 g TiO_2/100 m^2 Al_2O_3. When TiO_2 content was lower than this value, TiO_2 mainly deposited on the external surface of alumina with monolayer high dispersion state; whereas the TiO_2 content was larger than this value, TiO_2

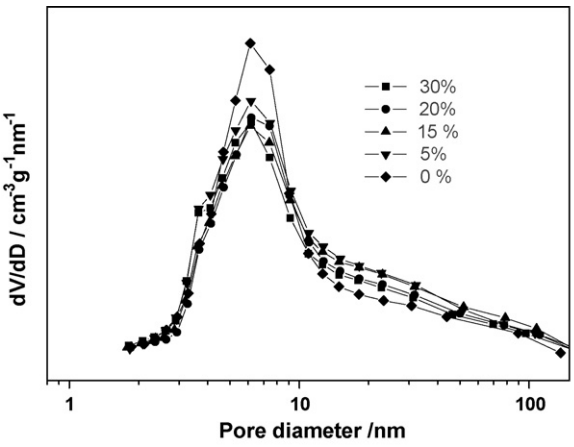

Fig. 1. Pore size distributions of NiMo/TiO_2-Al_2O_3 catalysts with different TiO_2 contents.

Table 2
Textural properties of NiMo/TiO_2-Al_2O_3 catalysts with different TiO_2 contents

Catalysts	TiO_2 (m%)	S_{BET} ($m^2 g^{-1}$)	V_{BJH} ($cm^3 g^{-1}$)	Average pore diameter (nm)
NiMo/TiO_2-Al_2O_3-1	0	252.3	0.56	8.82
NiMo/TiO_2-Al_2O_3-2	5	248.7	0.57	9.69
NiMo/TiO_2-Al_2O_3-4	15	223.9	0.60	10.17
NiMo/TiO_2-Al_2O_3-5	20	221.0	0.54	9.85
NiMo/TiO_2-Al_2O_3-7	30	231.1	0.54	9.28

Table 3
Textural properties of NiMo/TiO_2-Al_2O_3 sulfided catalysts with different TiO_2 contents after HDS reaction

Sulfided catalysts	TiO_2 (m%)	S_{BET} ($m^2\ g^{-1}$)	V_{BJH} ($cm^3\ g^{-1}$)	Average pore diameter (nm)
NiMo/TiO_2-Al_2O_3-1	0	163.5	0.40	8.95
NiMo/TiO_2-Al_2O_3-4	15	146.9	0.38	10.46
NiMo/TiO_2-Al_2O_3-7	30	123.2	0.29	9.45

congregated to be anatase crystal even to form Al_2TiO_5 phase. The incorporation of TiO_2 into Al_2O_3 system facilitated the formation of octahedral Mo species which is favorable for more CUS or sulfur vacancy active sites, and prohibited the formation of tetrahedral Mo species and $Al_2(MoO_4)_3$ configurations which possessed lower HDS activities [27,28,15].

In this paper, no Al_2TiO_5 was detected on the catalyst surface, conforming that the introduction of TiO_2 with proper proportion to Al_2O_3 can keep the pore volumes and average pore sizes of composite catalysts at high levels, which would facilitate the adsorption and diffusion of the large molecule including refractory components such as DBTs in diesel oil. From the data in Table 3, the specific surface areas and pore volumes of the sulfided catalysts decrease sharply after HDS reaction, which may be caused by the remains of feedstock residue. The average pore sizes of these catalysts are almost the same as their oxide precursors before HDS reaction (Fig. 1), implying that although the accumulation of TiO_2 results in the reduction of surface areas and pore volumes, the structures of composite catalysts keep at a stable state and no structural collapse occur during HDS reaction.

3.2. UV–vis DRS analysis

The UV–vis DRS is applied to determine the structures of TiO_2-Al_2O_3 binary oxides in the range from 200 to 800 nm as shown in Fig. 2. It can be observed that, compared with the pure γ-Al_2O_3, TiO_2-Al_2O_3 binary oxides show broad absorption bands of 220–265 and 320–355 nm. These bands are due to the $O^{2-} \rightarrow Ti^{4+}$ charge transfer transition corresponding to the excitation of electrons from the valence band (having the O 2p character) to the conduction band (having the Ti 3d character), which is the characteristic of anatase TiO_2 [29,30].

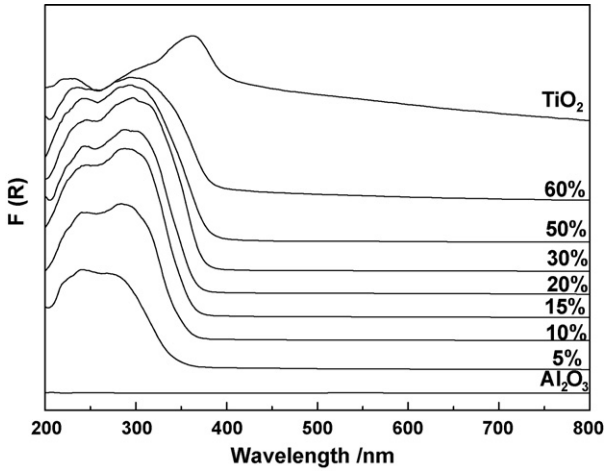

Fig. 2. UV–vis DR spectra of TiO_2-Al_2O_3 binary oxides with different TiO_2 contents.

Fig. 3 shows the UV–vis spectra of Ni-Mo/TiO_2-Al_2O_3 oxide catalysts base on the backgrounds of supports. Compared with the samples of Al_2O_3-supported catalysts, the absorption bands of titania-alumina supported molybdenum catalysts shift to the higher wavelengths (280–355 nm). The band at 220–250 nm is commonly attributed to the tetrahedral molybdate, whereas the band at 320 nm is assigned to the Mo–O–Mo bridge bond of the octahedral coordination [31–33]. In this paper, along with the TiO_2 loading increasing, the band at 220–250 nm disappears meaning that the tetrahedral molybdates reduce, but the band between 345 and 390 nm belonging to the octahedral coordination Mo species or MoO_3 crystal apparently shift to the longer wavelength and the intensity is becoming stronger, which indicate that the incorporation of TiO_2 weakens

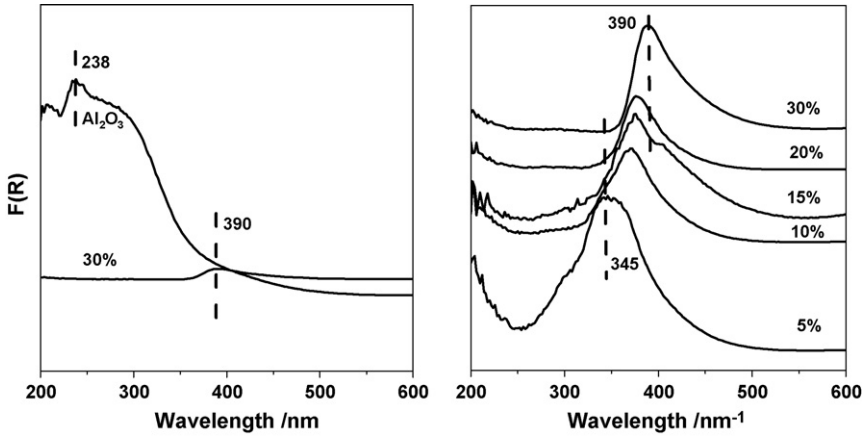

Fig. 3. UV–vis DR spectra of NiMo/TiO_2-Al_2O_3 catalysts with different TiO_2 contents.

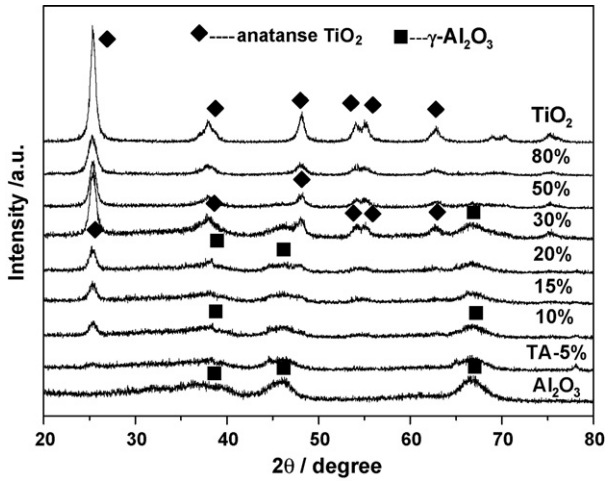

Fig. 4. XRD patterns of the TiO_2-Al_2O_3 binary oxides with different TiO_2 contents.

the support–metal interaction and is propitious to the formation of the octahedral Mo active species [34].

3.3. XRD analysis

Fig. 4 shows the XRD patterns of the TiO_2-Al_2O_3 binary oxide with different TiO_2 contents. From Fig. 4, it can be seen that, when the weight ratio of $TiO_2/(TiO_2 + Al_2O_3)$ is lower than 10%, the XRD patterns of the binary oxides show the typical reflections of crystallized γ-Al_2O_3. When the ratio exceeds 10%, the peaks of anatase TiO_2 can be observed at the 2θ of 25.3°, and the peak intensities also enhance with Ti contents. And when the ratio is up to 30%, the peaks of γ-Al_2O_3 at the 2θ of 38.5°, 46.3° and 66.7° disappear. At the same time, more typical peaks of anatase TiO_2 are present at 2θ of 39.0°, 48.1°, 62.9°, 54.0° and 55.1°, indicating the clusters of accumulated TiO_2 becoming larger, which are consilient to the BET results.

Fig. 5 shows the XRD patterns of the NiMo/TiO_2-Al_2O_3 catalysts with different TiO_2 contents. No typical peak of MoO_3 crystal is found, indicating that metal active component of Mo in the supported catalysts are highly dispersed. According to literature [35], it was not the rutile TiO_2 and the tialite (Al_2TiO_5), but the anatase TiO_2, which could weaken the interactions between the molybdate and TiO_2-Al_2O_3 supports. Combining the above UV–vis spectra of catalysts, it verifies that the molybdate species highly disperse on the anatase TiO_2 composite support and exist as octahedral coordination which facilitate the formation of coordinatively unsaturated or sulfur vacancies [36].

3.4. FT-Raman analysis

To verify the crystalline phase of TiO_2-Al_2O_3 binary oxides with different Ti contents and the dispersion of Mo supported on TiO_2-Al_2O_3 binary oxides, the FT-Raman spectra are also performed as shown in Fig. 6. According to the literatures [14,37], the bands at 146, 197, 398, 520 and 642 cm^{-1} are the characteristic bands of anatase TiO_2. And the bands at 220, 340, 667, 821 and 996 cm^{-1} are the characteristic bands of MoO_3. The bands at 284 and 718 cm^{-1} are the characteristic bands of MoO_2. The band at 960 cm^{-1} is attributed to the vibration of Mo=O bond of polymerized molybdate species interacting with the support [38,39]. From Fig. 6, it can be seen that the band at 146 cm^{-1} is very weak when the content of Ti is lower than 20 m%. With increasing Ti contents in binary oxides, the band becomes intense. There is no characteristic band of MoO_3 in Fig. 6, implying that Mo active phase are highly dispersed on composite supports, which is consistent with the results of XRD and UV–vis DRS.

3.5. TPR analysis

The TPR profiles of NiMo/TiO_2-Al_2O_3 catalysts are shown in Fig. 7. The decreases in the reduction temperatures from maximum of 720–682 K, with TiO_2 contents varying from 0 to 30 m%, verify the higher reducibility of molybdenum on Al_2O_3-TiO_2 support. It could be explained that the incorporation of

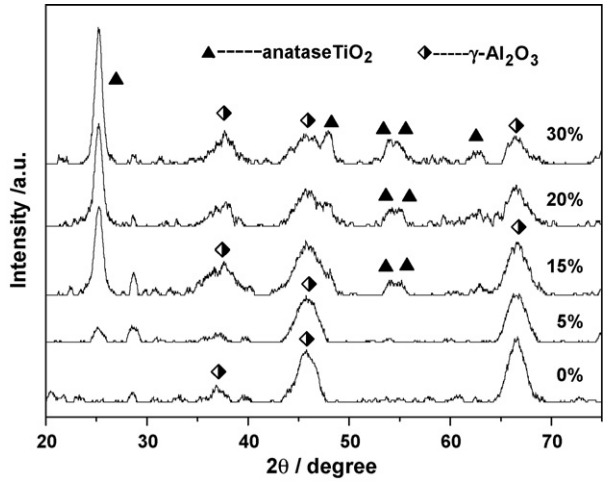

Fig. 5. XRD patterns of the NiMo/TiO_2-Al_2O_3 catalysts with different TiO_2 contents.

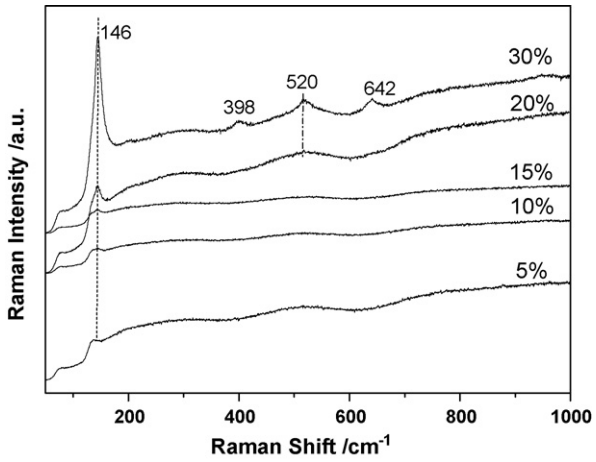

Fig. 6. FT-Raman spectra of NiMo/TiO_2-Al_2O_3 catalysts with different TiO_2 contents.

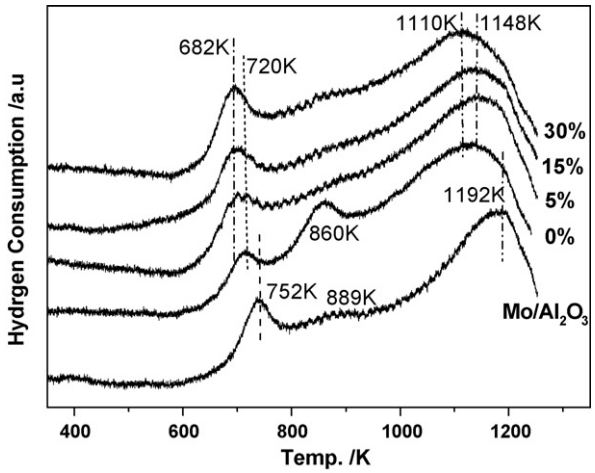

Fig. 7. TPR profiles of $NiMo/TiO_2$-Al_2O_3 catalysts with different TiO_2 contents.

TiO_2 into Al_2O_3 results in the weak SMI (support-metal interaction). It is known that the strong interaction between molybdena and alumina leads to the formation of more stable type of Mo^{4+} species. The less polarized bonds of polymolybdates are more easily reduced than those of the species directly bonded to alumina. The type of Mo^{6+} species in molybdenum catalysts depended on the composition of the support surface. The predominant polymolybdate species with octahedrally coordinated Mo^{6+} did not interact with the mixed supports as strong as in the case of alumina [40]. The polarization effect of Al^{3+} and Ti^{3+} ions produced in a reduction atmosphere may affect the covalency of Mo-O bonds and promote the reduction of Mo^{6+} to a lower valence states, such as Mo^{5+} or Mo^{4+}.

3.6. Pyridine FT-IR analysis

Table 4 gives the acid distributions of $NiMo/TiO_2$-Al_2O_3 catalysts by Py-FT-IR method. The incorporation of Ti to Al_2O_3 has a large effect on the acidic properties. For the samples of $NiMo/TiO_2$-Al_2O_3-χ ($\chi = 3$, 4 and 5), the amounts of Brönsted acid sites, Lewis acid sites and the total amounts of Brönsted acid and Lewis acid sites increase with the Ti content increasing. But the values of B/L ratios including weak and strong acid sites increase with the Ti contents, and keep at a relative higher value when TiO_2 content is 15 m%.

3.7. DRIFT spectra of NO adsorbed on the catalyst

Fig. 8a and b gives DRIFT spectra of NO adsorbed on catalysts with TiO_2 contents of 15 and 30% at different temperatures, respectively. Fig. 9a and b shows DRIFT spectra of NO adsorbed on the pure MoS_2 and the catalysts with TiO_2 contents of 15 and 30% at 303 and 473 K. From Fig. 8a and b, it can be seen that the band around 1650 cm^{-1} is assigned to the antisymmetric stretching vibration of dinitrosyl species adsorbed on CUS [41], and its intensity changes slowly with the increasing of temperature. From Fig. 9a and b, comparing with the DRIFT spectra of pure MoS_2 shown in the figures, the intensities of catalysts with TiO_2 loadings of 15 and 30% are higher than that of pure MoS_2, indicating that $NiMo/TiO_2$-Al_2O_3 catalysts possessed more coordinatively unsaturated sites. That is consistent with the results of XRD, UV–vis DRS and FT-Raman. Since pure MoS_2 is a coordinatively saturated chemical, the amounts of adsorbed NO may be due to the surface effect.

Table 4
Amounts of B and L acid sites determined by pyridine adsorption for $NiMo/TiO_2$-Al_2O_3 samples with different TiO_2 contents

Samples	TiO_2 (m%)	Amount of acid sites (μmol g^{-1}) (200 °C)				Amount of acid sites (μmol g^{-1}) (350 °C)			
		B	L	B + L	B/L	B	L	B + L	B/L
$NiMo/TiO_2$-Al_2O_3-2	5	1.63	15.69	17.02	0.085	1.60	1.26	2.86	1.27
$NiMo/TiO_2$-Al_2O_3-3	10	0.48	16.24	16.72	0.030	0.27	2.58	2.85	0.10
$NiMo/TiO_2$-Al_2O_3-4	15	0.85	20.19	21.04	0.042	0.43	4.23	4.66	0.11
$NiMo/TiO_2$-Al_2O_3-5	20	0.80	20.84	21.64	0.038	0.23	5.22	5.43	0.04

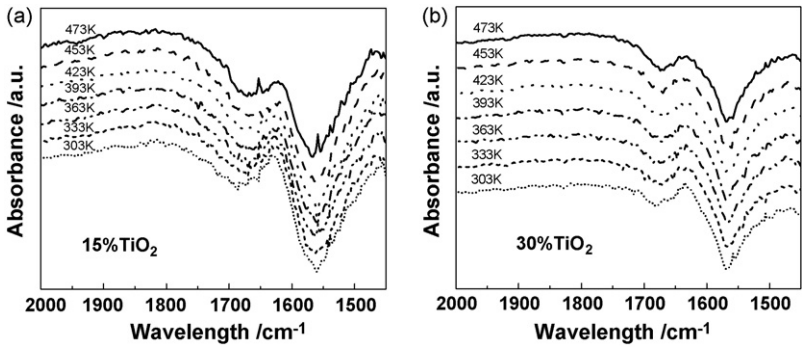

Fig. 8. DRIFT spectra of NO adsorbed on catalysts with TiO_2 contents of 15 and 30% at different temperatures.

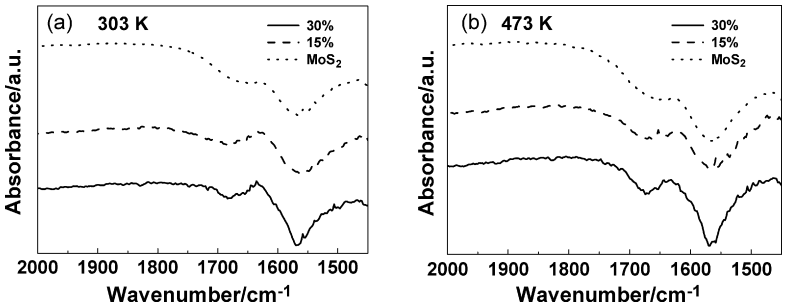

Fig. 9. DRIFT spectra of NO adsorbed on the MoS_2 and catalysts at 303 K (a) and 473 K (b).

3.8. Catalytic HDS activity

Table 5 and Fig. 10 show the sulfur distributions and HDS efficiencies of diesel feed over NiMo/TiO_2-Al_2O_3 catalysts. It can be found that the HDS efficiencies of catalysts increase with the Ti content increasing and reach a maximum value at TiO_2/(TiO_2 + Al_2O_3) ratio of 15%, as the total acidity reaches a high level (21.04 μmol g^{-1} at 200 °C and 4.66 μmol g^{-1} at 350 °C) and the B/L ratios at 200 and 350 °C are also relatively higher than those of the sample with TiO_2/(TiO_2 + Al_2O_3) ratio of 20 m%. Thus, the HDS efficiency of NiMo/TiO_2-Al_2O_3 catalysts with Ti content of 15% reaches 97.4%, which may be attributed to the higher reducibility of molybdenum on Al_2O_3-TiO_2 support, the higher CUS proportion and the relatively higher levels of total acidity and suitable B/L ratios of NiMo/TiO_2-Al_2O_3-15% catalyst. But with further increase Ti contents, the HDS efficiencies reduce due to the accumulation of TiO_2 crystal.

Table 5
HDS activities of NiMo/TiO_2-Al_2O_3 catalysts with different TiO_2 contents

	TiO_2 (m%)	S content (μg g^{-1})	HDS efficiency (%)
Feed		467.59	
NiMo/TiO_2-Al_2O_3-1	0	35.21	94.48
NiMo/TiO_2-Al_2O_3-2	5	21.32	95.52
NiMo/TiO_2-Al_2O_3-3	10	13.68	97.13
NiMo/TiO_2-Al_2O_3-4	15	13.16	97.24
NiMo/TiO_2-Al_2O_3-5	20	26.37	94.47
NiMo/TiO_2-Al_2O_3-6	25	30.68	93.57
NiMo/TiO_2-Al_2O_3-7	30	28.68	93.87

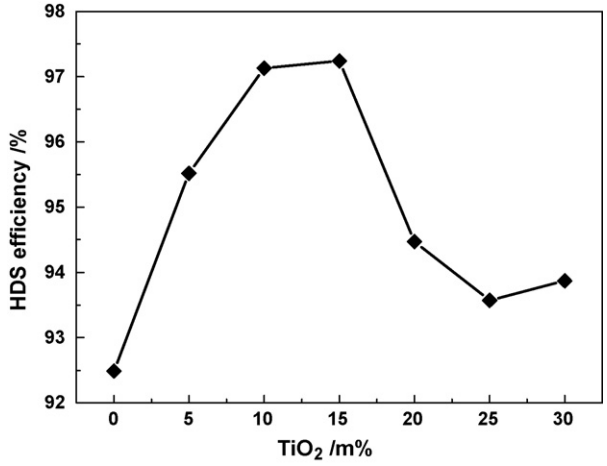

Fig. 10. The HDS activities of NiMo/TiO_2-Al_2O_3 catalysts with different TiO_2 contents.

From Fig. 10, the activities of NiMo catalysts supported on TiO_2-Al_2O_3 are all higher than that of the Al_2O_3-supported catalyst, the optimal HDS product in Table 5 can meet the sulfur regulation of Euro IV specification (<15 μg g^{-1}) of ultra clean diesel fuel.

4. Conclusions

In the present study, the blend of two commercial available diesels was hydrotreated over NiMo/TiO_2-Al_2O_3 catalysts with different Ti contents in order to investigate the roles of Ti incorporation into alumina by a sol–gel method. Based on the HDS activity results and catalyst characterization, it can be found that the anantase TiO_2 makes it easier to form octahedral coordination, which facilitates the formation of the coordinatively unsaturated sites or sulfur vacancies that are favorable for hydrodesulfurization reaction. Characterization results of UV–vis DRS, XRD, FT-Raman and H_2-TPR results verify that the incorporation of TiO_2 into Al_2O_3 support can adjust the interaction of support and active metal, and thus improve the reducibility of molybdenum on Al_2O_3-TiO_2 support. DRIFT spectra of NO adsorbed on the pure MoS_2 and the catalysts with TiO_2 loadings of 15 and 30% show that NiMo/TiO_2-Al_2O_3 catalysts possessed more coordinatively unsaturated sites. The result of Pyridine-FT-IR confirms that the relatively high total acidity amount and suitable B/L ratios of NiMo/TiO_2-Al_2O_3 catalysts facilitate the deep HDS reaction. The HDS efficiencies of catalysts increase with Ti contents and keep at high levels compared with the NiMo/Al_2O_3 sample. Furthermore HDS efficiency reaches a maximum at TiO_2/(TiO_2 + Al_2O_3) ratio of 15%, which is consistent with its higher reducibility of Al_2O_3-TiO_2 support, the higher CUS proportion and the suitable acidity distribution of NiMo/TiO_2-Al_2O_3-15% catalyst. The optimal HDS product can meet the sulfur regulations of Euro IV specification of ultra clean diesel fuel.

Acknowledgments

We acknowledge the financial supports from National Natural Science Foundation of China (No. 20406012), the

CNPC project (04A5050102 and 05E7019) and the 973 National Basic Research Program of China (Grant No. 2004CB217806).

References

[1] T.C. Ho, Catal. Today 98 (2004) 3.
[2] EPA, Control of air pollution from new motor vehicles: heavy-duty engine and vehicle standards and highway diesel fuel sulfur control requirements, Federal Register, vol. 66, 2001, p. 5101.
[3] H. Topsoe, B.S. Clausen, F.E. Massoth, in: J.R. Anderson, M. Boudart (Eds.), Catal. Sci. Techol. 11 (1996).
[4] M. Daage, R.R. Chianelli, J. Catal. 149 (1994) 414.
[5] G.M. Dhar, B.N. Snirivas, M.S. Rana, M. Kumar, S.K. Maity, Catal. Today 86 (2003) 45.
[6] S. Damyanoya, L. Petroy, M.A. Centeno, P. Grange, Appl. Catal. A 224 (2002) 271.
[7] J.R. Grzechowiak, J. Rynkowski, I.W. Zieliñska, Catal. Today 65 (2001) 225.
[8] C. Pophal, F. Kameda, K. Hoshino, S. Yoshinaka, K. Segawa, Catal. Today 39 (1997) 21.
[9] P. Rayo, J. Ancheyta, J. Ramírez, A.G. Alejandre, Catal. Today 98 (2004) 171.
[10] S.K. Maity, J. Ancheyta, L. Soberanis, F. Alonso, M.E. Flanos, Appl. Catal. A 244 (2003) 141.
[11] J.R. Grzechowiak, I.W. Zieliñska, K. Mrozińska, Catal. Today 119 (2007) 23.
[12] Z.B. Wei, Q. Xin, X.X. Guo, Appl. Catal. 63 (1990) 305.
[13] A.A. Cecílio, S.H. Pulcinell, C.V. Santilli, J. Sol–Gel Sci. Technol. 31 (2004) 87.
[14] Z.B. Wei, W.H. Yan, H. Zhang, T.L. Ren, Q. Xin, Z.C. Li, Appl. Catal. A 167 (1998) 39.
[15] R.G. Leliveld, A.J. Van, J. Catal. 117 (1997) 115.
[16] Y. Saih, K. Segawa, Catal. Surv. Asia 7 (2003) 235.
[17] Y. Saih, M. Nagata, T. Funamoto, Y. Masuyama, K. Segawa, Appl. Catal. A 295 (2005) 11.
[18] K. Segawa, M. Katsuta, F. Kameda, Catal. Today 29 (1996) 215.
[19] Y. Saih, M.A. Chaoui, A. Ezzamarty, M. Lakhdar, Catal. Commun. 2 (2001) 81.
[20] Y. Saih, K. Segawa, Catal. Today 86 (2003) 61.
[21] J. Ramírez, A.G. Alejandre, J. Catal. 170 (1997) 108.
[22] J. Ramírez, A.G. Alejandre, Catal. Today 43 (1998) 123.
[23] J. Ramírez, L. Cedeño, G. Busca, J. Catal. 184 (1999) 59.
[24] J. Ramírez, G. Macías, L. Cedeño, A.G. Alejandre, R. Cuevas, P. Castillo, Catal. Today 98 (2004) 19.
[25] J. Ramírez, P. Rayo, A.G. Alejandre, J. Ancheyta, M.S. Rana, Catal. Today 109 (2005) 54.
[26] C. Deng, L. Duan, C. Wang, J. Mol. Catal. 6 (1992) 15.
[27] Z.B. Wei, Q. Xin, X.X. Guo, Chin. J. Catal. 12 (1991) 255.
[28] Z.H. Luan, L. Kevan, Microporous Mesoporous Mater. 44 (2001) 337.
[29] A.G. Alejandre, J. Ramírez, G. Busca, Catal. Lett. 56 (1998) 29.
[30] S. Damyanova, A. Spojakina, K. Jiratova, Appl. Catal. A 125 (1995) 257.
[31] T. Klimova, M. Calderón, J. Ramírez, Appl. Catal. A 240 (2003) 29.
[32] M. Cheng, F. Kumata, T. Saito, T. Komatsu, Appl. Catal. A 183 (1999) 199.
[33] A.J. Duan, G.F. Wan, Z. Zhao, C.M. Xu, Y. Zheng, Y.G. Zhang, T. Dou, X.J. Bao, K. Chung, Catal. Today 119 (2007) 13.
[34] G. Xiong, C. Li, Z.C. Feng, P.L. Ying, Q. Xin, J.K. Liu, J. Catal. 186 (1999) 234.
[35] Y. Iwasawa, M. Yamagishi, J. Catal. 82 (1983) 373.
[36] H.Y. Zhu, M.M. Shen, Y. Wu, L.W. Xiao, J.M. Hong, B. Liu, X.L. Wu, L. Dong, Y. Chen, J. Phys. Chem. B 109 (2005) 11720.
[37] N. Shinichi, T. Yoshinori, A. Sachio, J. Mol. Struct. 441 (1998) 267.
[38] D.S. Zigg, L.E. Makovsky, R.E. Tischer, F.R. Brown, M. Hercules, J. Phys. Chem. 84 (1980) 2898.
[39] J.R. Grzechowiak, I.W. Zieliñska, Appl. Catal. A 250 (2003) 95.
[40] M. Yamada, N. Koizumi, M. Yamazaki, Catal. Today 50 (1999) 3.
[41] N. Koizumi, K. Takahashi, M. Yamazaki, M. Yamada, Catal. Today 45 (1998) 313.